Internal Proton Transfer and H−2 Rotations in the H−5(+) Cluster: A Marked Influence on Its Thermal Equilibrium State

ARTICLE *in* THE JOURNAL OF PHYSICAL CHEMISTRY A · MARCH 2011

Impact Factor: 2.69 · DOI: 10.1021/jp200392w · Source: PubMed

THE JOURNAL OF PHYSICAL CHEMISTRY A

ARTICLE

pubs.acs.org/JPCA

Internal Proton Transfer and H_2 Rotations in the H_5^+ Cluster: A Marked Influence on Its Thermal Equilibrium State

Ricardo Pérez de Tudela, Patricia Barragán, Rita Prosmiti,* Pablo Villarreal, and Gerardo Delgado-Barrio

Instituto de Física Fundamental, CSIC, Serrano 123, 28006 Madrid, Spain

ABSTRACT: Classical and path integral Monte Carlo (CMC, PIMC) "on the fly" calculations are carried out to investigate anharmonic quantum effects on the thermal equilibrium structure of the H_5^+ cluster. The idea to follow in our computations is based on using a combination of the above-mentioned nuclear classical and quantum statistical methods, and first-principles density functional (DFT) electronic structure calculations. The interaction energies are computed within the DFT framework using the B3(H) hybrid functional, specially designed for hydrogen-only systems. The global minimum of the potential is predicted to be a nonplanar configuration of C_{2v} symmetry, while the next three low-lying stationary points on the surface correspond to extremely low-energy barriers for the internal proton transfer and to the rotation of the H_2 molecules, around the C_2 axis of H_5^+, connecting the symmetric C_{2v} minima in the planar and nonplanar orientations. On the basis of full-dimensional converged PIMC calculations, results on the quantum vibrational zero-point energy (ZPE) and state of H_5^+ are reported at a low temperature of 10 K, and the influence of the above-mentioned topological features of the surface on its probability distributions is clearly demonstrated.

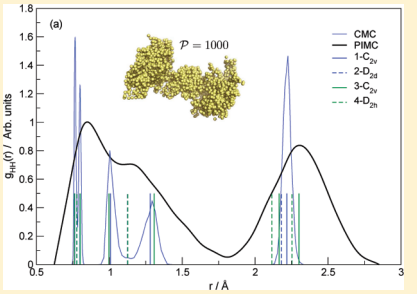

I. INTRODUCTION

H_5^+ is the first member of the H_{2n+1}^+ (with $n > 1$) series, and since its detection in 1962[1] it has been the subject of a plethora of experimental and theoretical studies. On the one hand, experimental observations are rather limited to a few vibrational frequencies (such as the fundamental stretching modes of H_3^+ and H_2 in H_5^+,[2] overtones of the H_3^+ stretching modes, or combinations of them with the intermolecular $H_3^+-H_2$ stretching mode,[3] and later on combination bands or overtones of the shared-proton stretch mode[4]), dissociation enthalpies for the $H_3^+ + H_2 \rightarrow H_5^+$ clustering reaction,[5−7] and, more recently, rate coefficients at typical interstellar clouds temperatures (5−50 K) have been reported.[8,9] On the other hand, theoretical predictions have been mainly focused on a local description of its potential energy surface, for example, minima and saddle-points, and only recently more accurate global analytical potentials have been reported in the literature.[10−13] It has been found that the potential energy surface of H_5^+ is very flat, and highly anharmonic around the global C_{2v} minimum with several low-lying saddle-points. This indicates a delocalized nature of H_5^+, and thus quantum effects should be considered as they are expected to be important on the zero-point energy and state of the H_5^+. Given the experimental difficulties to spectroscopic characterization of H_5^+, as well as its important role in the reaction mechanism of the deuterium fractionation in interstellar clouds,[14] further investigations in these directions are of particular interest.

So far, three studies in the literature have explored nuclear quantum effects and thermal contributions to the ground vibrational state of H_5^+.[15−17] The earlier one by Štich et al.[15] is based on an ab initio path integral molecular dynamics (PIMD) method combined with the Car−Parrinello[18] one. However, their DFT approach has failed to describe even qualitatively the H_5^+ surface. Later, Ohta et al.[16] have applied the PIMD method, employing the MP2 level of theory for the electronic structure calculations, and equilibrium structures for H_5^+ have been reported at different temperatures. The latter has provided more accurate results than the previous DFT ones,[15] however, only on structural features. More recently, diffusion Monte Carlo (DMC) calculations have shown that the zero-point averaged structure of the H_5^+ corresponds to an ideal D_{2d} symmetry,[17] with the proton in the middle of the two H_2 diatoms, and an anharmonic dissociation energy, D_0, value of 6.37 ± 0.01 kcal/mol for H_5^+ has also been reported. To date, the only data available on the anharmonic quantum effects for H_5^+ come for the above-mentioned DMC calculations using the analytical CCSD(T) surface by Xie et al.[12] However, the parametrized surface used in the DMC study presents oscillatory artifacts for distorted $H_3^+-H_2$ geometries nearby the minima of the surface, as well as its asymptotes (see refs 13,22). A key point for carrying out a reliable study is the description of the underlying potential energy surface; thus, we think that H_5^+ should be revisited by employing a realistic surface.

Because the full quantum mechanical calculations of H_5^+ are beyond current capabilities, insights on anharmonic quantum and thermal effects obtained from quantum statistical approaches will be helpful in guiding future studies. In the present study, we aim to characterize the thermal equilibrium state of H_5^+ by performing "on the fly" (direct) CMC and full-dimensional converged PIMC calculations within the DFT framework, using

Received: January 14, 2011
Revised: February 16, 2011
Published: March 10, 2011

Table 1. Total Energy (in au) for the 1-C_{2v} Global Minimum Structure and Relative Energies (in kcal/mol) for the Next Three Low-Lying H_5^+ Optimized Conformers Predicted by the DFT/B3(H) Calculations Using cc-pVTZ and cc-pVQZ Basis Sets[a]

conformer	B3(H)/VTZ	B3(H)/VQZ[22]	CCSD(T)-R12[21]	CCSD(T)[10]	PES[12]	PES[11]
1-C_{2v}	−2.531515	−2.532656	−2.531794	−2.530509	−2.528015	−2.518215
2-D_{2d}	0.058	0.09	0.176	0.183	0.149	0.080
3-C_{2v}	0.296	0.302	0.276	0.273	0.294	0.256
4-D_{2h}	0.392	0.483	0.521	0.5210	0.458	0.419

[a] Results from previous high levels calculations and PESs are also listed.

Table 2. Harmonic Vibrational Frequencies (in cm^{-1}) for 1-C_{2v}, 2-D_{2d}, 3-C_{2v}, and 4-D_{2h} Conformers of H_5^+ Calculated at the B3(H)/cc-pVTZ Level of Theory, and Compared (in Parentheses) to the Ones from the Analytical PES by Xie et al.[12a][a]

mode	1-C_{2v}	2-D_{2d}	3-C_{2v}	4-D_{2h}
1	216 (211) A_2	−399 (503) B_2	−212 (−211) A_2	−453 (−508) B_1''
2	447 (487) A_1	229 (217) B_1	477 (474) A_1	−227 (−217) A''
3	884 (829) B_2	967 (971) E	821 (795) B_2	897 (906) B_2''
4	916 (882) B_1	967 (971) E	1066 (1011) B_1	1156 (1147) B_3''
5	1295 (1190) B_1	1415 (1430) A_1	1110 (1041) B_2	1328 (1346) B_3'
6	1649 (1799) A_1	1613 (1616) E	1713 (1824) A_1	1416 (1418) A'
7	1996 (2128) B_2	1613 (1616) E	2058 (2151) B_2	1761 (1761) B_2''
8	3833 (3666) A_1	3994 (3861) B_2	3817 (3658) A_1	4002 (3858) B_1''
9	4199 (4091) A_1	4081 (3924) A_1	4229 (4086) A_1	4102 (3912) A'

[a] The number of the negative values indicates the order of the saddle-point.

the B3(H) hybrid functional specially designed for hydrogen-only systems.[19] Such an alternative approach provides us with a realistic and relatively low computational cost DFT surface without any posterior parametrization procedure. Thus, our goal is to resolve issues such as floppiness and anharmonicity of the H_5^+ surface, and to assess the importance of quantum effects on the vibrational ground state, which are expected to be significant even at low temperatures.

This Article is organized as follows. In section II, we describe the computational details and results obtained from the electronic structure calculations, together with the ones from the classical and PIMD simulations. In this section, we also present comparisons with available experimental data, while some conclusions are given in section III.

II. COMPUTATIONAL DETAILS AND RESULTS

A. Electronic Structure Calculations. Here, all electronic structure calculations are performed with the Gaussian 03 software package.[20] As a first step, to present the accuracy of the DFT/B3(H) approach, we list in Table 1 comparisons with results obtained from previous studies at different levels of theory, such as MP2, CCSD(T), and CC-R12, for the four low-lying stationary points on the H_5^+ surface.[10,11,21,22] For reasons of comparison, DFT calculations are shown with both cc-pVTZ and cc-pVQZ basis sets. One can see that DFT calculations with the B3(H) functional reproduce their structure and energetics in an excellent agreement with the CC results. In particular, all of them are lying within an energy range of 0.4 kcal/mol above the minimum as compared to 0.5 kcal/mol predicted by the benchmark CC-R12 data. The relative order and the energy differences between them are also in accord with the high accurate CC-R12 results.[21]

Further, harmonic frequency analysis from B3(H)/cc-pVTZ calculations (see Table 2) shows that the lowest stationary point corresponds to a minimum, while the next three are first- and second-order saddle-points in absolute accord with the CC results.[10,25] In Figure 1, we show the four low-lying stationary points on the H_5^+ surface, together with the minimum energy path between the two conformers 1-C_{2v}/2-D_{2d} and 3-C_{2v}/4-D_{2h} for nonplanar and planar configurations, respectively, at MP2, CCSD(T), and DFT/B3(H) levels of theory using in all of them the cc-pVTZ basis set. The 2-D_{2d} and 4-D_{2h} conformers are the transition states corresponding to the internal proton transfer for nonplanar and planar configurations, respectively, while the 3-C_{2v} is the transition state for the HH interconversion in the H_2 moiety of the H_5^+. In Figure 1a,b, the x-axis shows the position of the proton by keeping fixed the distance between the centers of mass of the two H_2 molecules for nonplanar (see Figure 1a) and planar (see Figure 1b) configurations. In contrast, in Figure 1c the intermolecular distance R between the H_2 centers of masses varies, and in this case the position of the proton is fixed in the middle of each R value considering only 2-D_{2d} orientations for the H_5^+. For all panels of Figure 1, the y-axis corresponds to the optimized energies (total energies for each curve are shifted to their minimum value corresponding to level of theory) of these H_5^+ geometries at the indicated levels of theory. As we can see, the DFT/B3(H) calculations clearly describe all aspects of the potential in an excellent agreement with the CCSD(T) ones. We should note that the positions of minima and saddle-points are the same, although the CCSD(T) curve shows a higher barrier for the proton transfer and is slightly more anharmonic than the DFT/B3(H) one, and less anharmonic as compared to the MP2 results, for both nonplanar and planar configurations. By comparing now the energies as a function of the intermolecular R distance, we obtain an even better agreement between the CCSD(T) and DFT/B3(H) computations. Concerning now the dissociation of the H_5^+ to $H_3^+ + H_2$, the B3(H)/cc-pVTZ surface predicts a D_e energy value of 9.44 kcal/mol. Previous theoretical studies have estimated values of 7.70 and 7.84 kcal/mol from

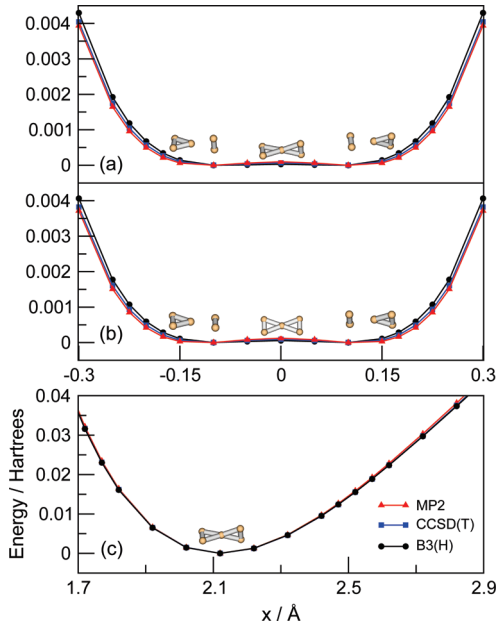

Figure 1. Optimal energies for H_5^+ obtained at indicated levels using the cc-pVTZ basis set. For comparison reasons, the corresponding curves for each level of theory are shifted to their minimum total energy values. In the top panels, the distance of the center of masses of the two H_2 monomers and the orientation of the H_5^+ are fixed at the ones of (a) the 2-D_{2d} and (b) 4-D_{2h} configurations, while in the bottom one (c) the distance between the H_2 centers of masses varies, by keeping fixed the proton in its middle for 2-D_{2d} orientations of H_5^+. In the inset of each panel, the corresponding orientations of minima and saddle-point are also shown.

MP2 and MP4 calculations,[11,23] 8.90 kcal/mol at G2(MP2) level,[24] and 8.58, 8.65 kcal/mol from accurate CC-R12 and CCSD(T)/CBS calculations, respectively.[21,25] A more detailed study on the DFT/B3(H) surfaces is given in refs 22,26.

On the basis of all of these comparisons, we conclude that DFT/B3(H) yields an accurate description of the potential of H_5^+. Thus, we consider the implementations of this level for the electronic state calculation in the ab initio classical MC and PIMC methods described below.

B. Classical and Path-Integral Monte Carlo: "On the Fly" Simulations. As mentioned above, the four lowest stationary points of the potential surface of H_5^+ are lying very close in energy, within ~0.5 kcal/mol, and the region around them is extremely flat and anharmonic. Also, given the light mass of the H atoms, quantum effects are expected to be important in the characterization of its ground vibrational state. For studying molecules that undergo large-amplitude motions, quantum approaches are required, although given the number of atoms, such full-dimensional treatments of the H_5^+ dynamics are still challenging. An alternative approach to address these issues is to use the PIMC formalism. This method is a treatment of quantum nature, going beyond standard harmonic mode analysis.[27] It is based on a statistical mechanics approach to the molecular system and has been applied to calculate thermochemical properties.[28,29]

Briefly, to compute the thermal average of the property $\mathcal{A}$, the following expression must be evaluated:

$$\langle A \rangle = Z^{-1} \int \mathrm{d}R\, \mathrm{d}R'\, \rho(R,R';\beta)\langle R|\mathcal{A}|R'\rangle \qquad (1)$$

where $Z = \int \mathrm{d}R\, \rho(R,R;\beta)$ is the partition function, and $\rho(R,R';\beta) = \langle R|e^{-\beta\hat{\mathcal{H}}}|R'\rangle$ is the density matrix of the system at a temperature $T = 1/k_B\beta$, with $\hat{\mathcal{H}}$ being the Hamiltonian.

The path integral Monte Carlo method[28] makes use of a convolution property that allows the density matrix of a quantum system of N particles at a temperature T to be computed as a multidimensional integral of the product of $\mathcal{P}$ density matrices at a higher temperature T:

$$\rho(R,R';\beta) = \int \mathrm{d}R_1 \ldots \mathrm{d}R_{\mathcal{P}-1}\, \rho(R,R_1;\beta/\mathcal{P}) \ldots \rho(R_{\mathcal{P}-1},R';\beta/\mathcal{P}) \qquad (2)$$

Several approximations[30−32] can be made in these new $\rho(R,R_1;\beta/\mathcal{P})$ density matrices, the most trivial being the so-called primitive approximation, where the commutator between the kinetic and the potential operators is neglected, which leads to a complete separation between kinetic ρ_{free} and potential ρ_V density matrices:

$$\rho_{\mathrm{free}}(R_i,R_j;\beta/\mathcal{P}) = \left(\frac{4\pi\hbar^2\beta}{2m\mathcal{P}}\right)^{-3N/2} \exp\left[-\frac{2m\mathcal{P}}{4\hbar^2\beta}(R_i-R_j)^2\right]$$
$$\rho_V(R_i,R_j;\beta/\mathcal{P}) = \delta(R_i-R_j)e^{-(\beta/\mathcal{P})V(R_i)} \qquad (3)$$

The multidimensional integrals involved in eq 1 are carried out using the Monte Carlo method that samples the configurational space following a probability density function defined as the product of the density matrices in eq 3. A particularly effective sampling technique called staging[33] is used to perform smart collective bead movements (within the classical isomorphism) that directly sample the kinetic part, using a Metropolis[34] algorithm for the potential part.

All calculations are performed at a temperature of T = 10 K, a typical interstellar clouds value, for evaluating mainly the anharmonic quantum effects for H_5^+ at DFT/B3(H) level of theory. Several test runs are carried out to check the efficiency of the configuration space sampling for the equilibration. We found that the staging[33] method was essential to reach the thermal equilibrium state within a few tens of thousands of potential evaluations. Also, particular attention has been paid to the convergence with the number of beads, as well as the total number of configurations to obtain convergence of the properties of interest. Therefore, a total of 60 000 MC steps, after equilibration, are carried out using $\mathcal{P}$ = 1000 beads per atom to achieve convergence in the quantum PIMC computations (see below). Given the large number of beads, test runs were carried out by employing two fundamentally different kinetic energy estimators (thermodynamic and virial ones[35,36]), and both of them yield almost identical values. We should note that the combination of the primitive factorization scheme used for the path integral representation of the density matrix and the performance of the thermodynamic estimator allows us to avoid the expensive cost of force evaluations, and to keep our simulations in a reasonable CPU time. In this way, both classical and quantum distribution functions for H_5^+ at 10 K are obtained. First, in Figure 2a we present the HH radial pair distribution function, where one can see that the classical one presents five sharp peaks, well localized around the optimized HH bond distances of the 1-C_{2v} at the DFT/B3(H) levels of theory (see vertical bar lines in Figure 2a). In contrast, the quantum calculation yields at the same temperature substantially broader peaks, indicating that the cluster expands in the configuration space, and quantum tunneling occurs

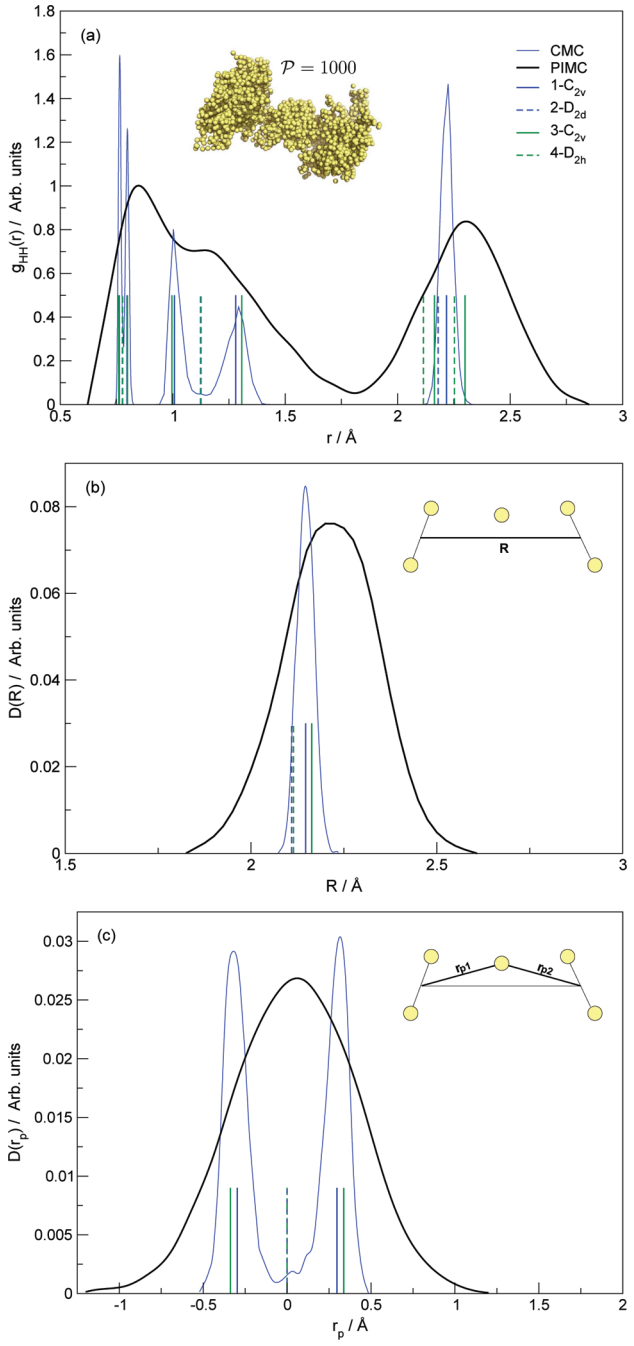

Figure 2. Classical and quantum radial distribution functions at T = 10 K for H_5^+, as a function of (a) r, (b) R, and (c) r_p. The vertical solid lines indicate the optimized at DFT/B3(H) level HH bond lengths for the 1-C_{2v}, 2-D_{2d}, 3-C_{2v}, and 4-D_{2h} structures. In the inset of the top panel (a), we present a snapshot of the last MC step of the PIMC calculation of H_5^+, while in the (b,c) panels the corresponding coordinates are demonstrated.

between the two equivalent 1-C_{2v} structures via internal proton transfer. In particular, the classical first double-peak attributed to the two H_2 distances in H_5^+ is substituted by a quantum broader one in the range of about 0.7−1.0 Å. The next one is even wider, covering HH distances from 1.0 to 1.4 Å, while the last one is slightly shifted to longer HH bond lengths, at 2.3 Å, than the classical one at 2.23 Å. These remarkable changes in the radial

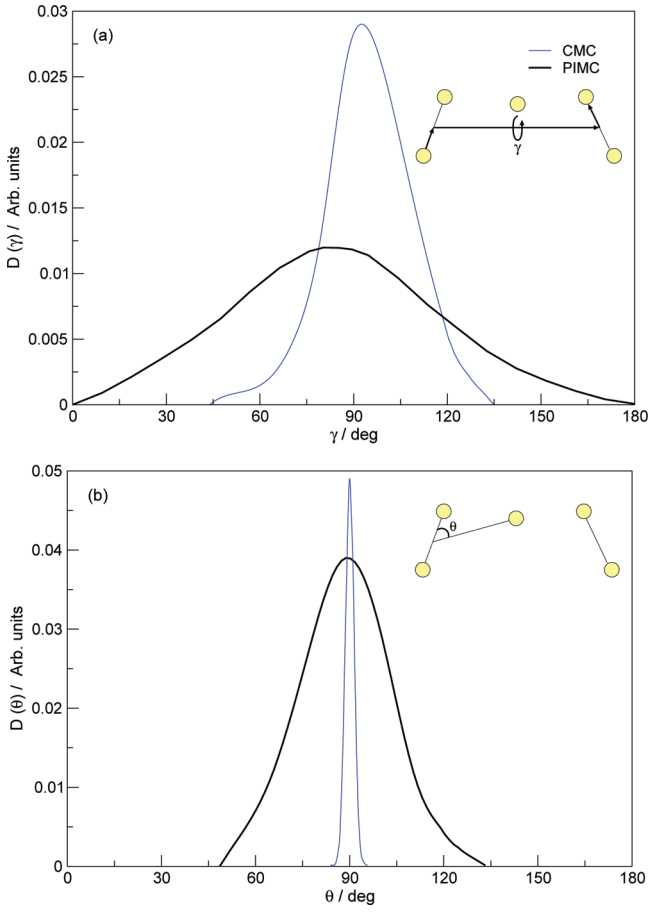

Figure 3. Classical and quantum (a) D_γ and (b) D_θ angular distribution functions at T = 10 K for H_5^+. In the inset of each panel, the corresponding angle is shown.

distributions indicate the quantum delocalization of the central proton. For comparison reasons, we also plot in Figure 2a the optimized HH bond distances of the 2-D_{2d}, 3-C_{2v}, and 4-D_{2h} stationary points of H_5^+ obtained from the DFT/B3(H) calculations. Also, in the inset of the figure, we show a view of the H_5^+ during the last MC step of our PIMC simulation. As one can see, the quantum ground state of H_5^+ corresponds to a mixture of all these four low-lying conformers.

In Figure 2b and c, classical and quantum distribution functions as a function of the intermolecular distance, R, between the center of masses of the two H_2 units, and r_p, which is given as the difference of the distances r_{p1} and r_{p2} of the proton from each H_2 center of mass (refer to the inset of Figure 2c for definition), are depicted. Again, the classical ones are both located around the geometry of the global 1-C_{2v} minimum, with a double-peak for the $D(r_p)$ distribution due to the two symmetric 1-C_{2v} wells in this coordinate. In contrast, the quantum ones are more extended in the configuration space with $D(R)$ presenting a maximum at larger R values of about 2.2 Å. For the $D(r_p)$ distribution, the maximum density is obtained now for the geometries corresponding to the 2-D_{2d} and 4-D_{2h} conformers of H_5^+. The height of the barrier of the double-well potential depends on the R distance, and the proton transfer occurs for R distances from around 2.0 to 2.5 Å. As R increases, the potential barrier is getting higher, as it was expected for describing at the end the asymptotic $H_3^+ + H_2$ limit (see also Figure 1c).

dx.doi.org/10.1021/jp200392w |J. Phys. Chem. A 2011, 115, 2483–2488

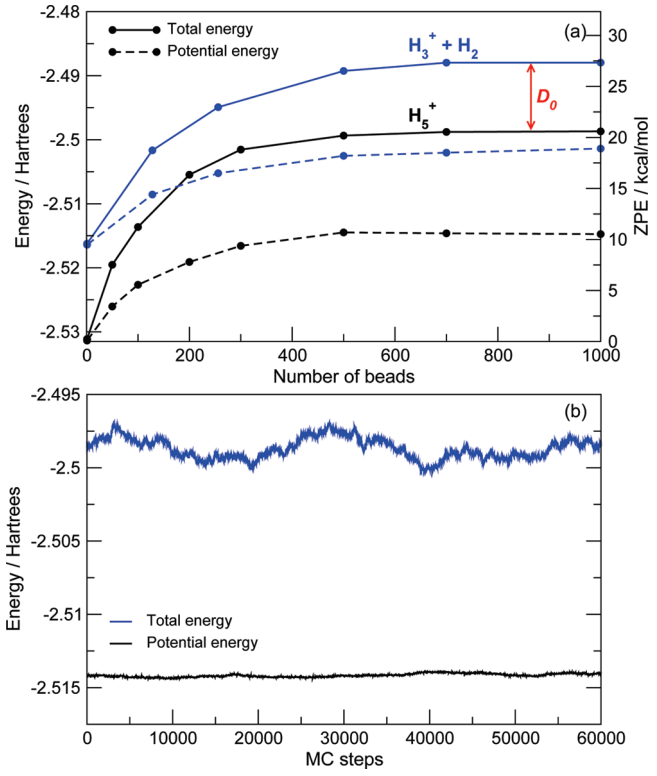

Figure 4. Potential and total energy values for H_5^+ and $H_3^+ + H_2$ at 10 K from the PIMC simulations, as a function of (a) number of beads and (b) number of Monte Carlo steps with $\boldsymbol{P}$ = 1000 for H_5^+. Statistical errors are smaller than the size of the circle symbols.

To further investigate quantum effects, such as internal H_2 rotations, on the zero-point motions of H_5^+ angular distribution functions are also obtained. Figure 3 shows such calculated distributions, $D(\gamma)$, where γ is the dihedral angle defined by three sequential noncollinear vectors (two of them are the ones connecting one H-atom of one H_2 unit with its center of mass, and then the one between the two center of masses of the two H_2 monomers) (see Figure 3a), and $D(\theta)$, with θ being the angle formed by the vector along the one H_2 unit, and the one connecting its center of mass and the central proton (see Figure 3b). This angle corresponds to the H_3^+ bending motion, while the angle γ describes the rotation of the H_2 units. Both classical distributions are well localized around the value of 90°, while the quantum ones are completely different each other. The quantum $D(\theta)$ is remarkably broader than the classical one, whereas the $D(\gamma)$ one is extended over the whole range, indicating a free rotation of the H_2 molecules around the C_2 axis of H_5^+. On the basis of these results, we conclude that the vibrational ground state of the H_5^+ is consistent with a combination of its four lower-lying structures, 1-C_{2v}, 2-D_{2d}, 3-C_{2v}, and 4-D_{2h}, and not only of the D_{2d} one as it has been recently claimed from DMC calculations.[17]

From the present PIMC calculations, the thermal equilibrium state energy and the corresponding anharmonic dissociation energy/enthalpy for H_5^+ are also predicted. In Figure 4a, we plot the averages of the potential (given by the B3(H) calculations) and the total energies, obtained using the thermodynamic kinetic energy estimator,[35] for H_5^+ and $H_3^+ + H_2$ as a function of the number of beads. One can see that a value of P = 500 beads is sufficient to converge potential values (structural features), while

Table 3. Experimental and Theoretical Dissociation Energies/Enthalpies of $H_5^+ \rightarrow H_3^+ + H_2$[a]

expt/theor	D_e/kcal/mol	T/K	$\Delta H(T)$/kcal/mol
Beuhler et al. (1983)[5]	n/a	25−330	6.6 ± 0.3
Hiraoka (1987)[6]	n/a	25−330	6.9 ± 0.3
Hiraoka, Mori (1989)[7]	n/a	25−330	7.0 ± 0.1
Cheng et al. (2010)[4]	n/a	n/a	≤7.44
Ohta et al. (2004)[16]/PIMD-MP2	7.70	5−200	n/a
Xie et al. (2005)[12]/DMC	8.30	0.0	6.33 ± 0.03
Acioli et al. (2008)[17]/DMC	8.30	0.0	6.37 ± 0.01
This work/PIMC-DFT	9.44	10	7.02 ± 0.36

[a] Available well-depths, D_e, are also listed.

to achieve convergence for the total energy at least 900 beads are needed in the PIMC calculations for H_5^+ at T = 10 K. In Figure 4b, we present the evolution of potential and total energy terms for H_5^+ during the last 60 000 steps of the quantum PIMC simulation with $\boldsymbol{P}$ = 1000, which is used in our analysis. On the basis of these PIMC results, average zero-point energies of 20.60 ± 0.15 and 27.62 ± 0.21 kcal/mol are obtained for H_5^+ and $H_3^+ + H_2$ fragments, respectively (see also Figure 4a). The errors are estimated following the standard statistical error analysis procedure for correlated data.[37] In turn, an anharmonic dissociation energy value D_0 = 7.02 ± 0.36 kcal/mol at 10 K is also calculated, with thermal corrections counting to about $RT \approx$ 0.02 kcal/mol, where R is the molecular gas constant.

In Table 3, we present comparisons with results available from previous experimental and theoretical studies. In comparison with the D_0 value of 6.37 kcal/mol from the recent DMC calculations,[17] the present study predicts somehow higher value, due to the underlying PES employed. The difference in the D_0 may be attributed mainly to the deeper potential well predicted by the DFT/B3(H) surface than the analytical potential by Xie et al.[12] used in the DMC calculations.[17] Also, as we have mentioned above, this analytical PES presents serious artifacts, and such behavior of the surface might affect quantitatively the results obtained by the previous DMC calculations that rely on it,[17] because these shortcomings appear at configurations nearby the potential minima and asymptotes.[13,22,38] One can see that the present estimate for the D_0 energy is closer to the experimental upper limit of 7.44 kcal/mol reported recently by Cheng et al.,[4] from the IR photodissociation spectrum of H_5^+, and also is in very good agreement with the earlier experimental data[5−7] on dissociation enthalpies, over the range of temperature of 25−330 K, for $H_5^+ \rightarrow H_3^+ + H_2$ reaction of 6.6 ± 0.3, 6.9 ± 0.3, and 7.0 ± 0.1 kcal/mol, respectively.

Further, as we mentioned above, we estimated from the PIMC calculation a fully converged anharmonic ZPE of 7204.9 cm^{-1} for H_5^+, while within the harmonic approximation at the DFT/B3(H) level of theory a value of 7717.5 cm^{-1} is obtained from the values in Table 2. As we can see, a significantly large anharmonicity of 513 cm^{-1} (1.47 kcal/mol) is found for H_5^+. The best estimates of the harmonic ZPE from MP2 and CCSD-(T) calculations are 7834.5 and 7650.5 cm^{-1}, respectively.[25] These results compare well with those from two previous studies available on the anharmonic ZPE of H_5^+. In particular, from an earlier study on the anharmonic vibrational frequencies of H_5^+ using the MP2-VSCF approximation, a value of 7403 cm^{-1} has been reported,[39] while from a recent one based on DMC calculations[17] using the Xie et al. surface,[12] values of 7208 and

434 cm^{-1} (1.24 kcal/mol) have been predicted for the ZPE and the anharmonicity of H_5^+, respectively. Comparison with the available experimental data and previous theoretical results, where harmonic approximation has been employed[22] to obtain the D_0 and ZPE values, indicates the importance of rigorous theoretical calculations that include correctly the anharmonicity of the H_5^+ PES, where nuclear quantum effects are particularly important.

III. CONCLUSIONS

In summary, we first show that DFT/B3(H)-based electronic structure calculations yield an accurate overall representation of the H_5^+ surface at relative low computational cost, able to describe for first time (within a DFT formalism) the interconversion of the central proton transfer. On the other hand, we demonstrated (by comparing with classical MC results) the importance of the nuclear quantum anharmonic effect on the structural zero-point state of H_5^+ based on converged full-dimensional PIMC "on the fly" calculations using the DFT/B3(H) surface. At 10 K, the H_5^+ probability density distributions show a free intermolecular transfer of the central proton between the two H_2 molecules, which are almost freely rotating around the C_2 axis of H_5^+. This finding indicates that the thermal equilibrium state of H_5^+ corresponds to the four low-lying minima of the surface, 1-C_{2v}, 2-D_{2d}, 3-C_{2v} and 4-D_{2h} and does not have an ideal 2-D_{2d} symmetry as it has been predicted for the ground vibrational state by the DMC calculations.[17] The binding energy value obtained from the present PIMC simulations is closer to the experimental data available, and our results indicate that quantum treatments are necessary for determining the molecular structure and dissociation enthalpy of this cluster.

Because the H_5^+ complex plays a key role in the reaction mechanism of the deuterium fractionation in interstellar medium,[8] and because H_5^+ is the simplest model system including internal proton transfer for studying proton and hydrogen transport in hydrogen storage systems,[40] the present calculations may provide accurate means to explore the underlying mechanisms in astrophysical and technological applications. Furthermore, the approaches employed, together with the information obtained, are expected to be particularly useful for studying properties of larger clusters of this H_{2n+1}^+ series, for example, solvation effects, cluster fragmentation, and collision processes related to the interstellar chemistry reactions. We will urge the use of such an approach in future modeling studies.

AUTHOR INFORMATION

Corresponding Author
*E-mail: rita@iff.csic.es.

ACKNOWLEDGMENT

Support by CSIC, Grant No. PIE-2008501085, DGICYT, Spain, Grant Nos. FIS2007-62002, FIS2010-18132, and MICINN: Consolider, Grant No. CSD2009-00038 is gratefully acknowledged. We thank the Centro de Calculo (IFF), CTI (CSIC), and CESGA for allocation of computer time.

REFERENCES

(1) Dawson, P. H.; Thickner, A. W. *J. Chem. Phys.* **1962**, *37*, 672.
(2) Okumura, M.; Yeh, L. I.; Lee, Y. T. *J. Chem. Phys.* **1998**, *88*, 79.
(3) Bae, Y. K. *Chem. Phys. Lett.* **1991**, *180*, 179.
(4) Cheng, T. C.; Bandyopadyay, B.; Wang, Y.; Carter, S.; Braams, B. J.; Bowman, J. M.; Duncan, M. A. *J. Phys. Chem. Lett.* **2010**, *1*, 758.
(5) Beuhler, R. J.; Ehrenson, S.; Friedman, L. *J. Chem. Phys.* **1983**, *79*, 5982.
(6) Hiraoka, K. *J. Chem. Phys.* **1987**, *87*, 4048.
(7) Hiraoka, K.; Mori, T. *J. Chem. Phys.* **1989**, *91*, 4821.
(8) Gerlich, D.; Windisch, F.; Hlavenka, P.; Plašil, R.; Glosik, J. *Philos. Trans. R. Soc. London, Ser. A* **2006**, *364*, 3007.
(9) Hugo, E.; Asvany, O.; Schlemmer, S. *J. Chem. Phys.* **2009**, *130*, 164302.
(10) Prosmiti, R.; Buchachenko, A. A.; Villarreal, P.; Delgado-Barrio, G. *Theor. Chem. Acc.* **2001**, *106*, 426.
(11) Moyano, G. E.; Collins, M. A. *J. Chem. Phys.* **2003**, *119*, 5510.
(12) Xie, Z.; Braams, B. J.; Bowman, J. M. *J. Chem. Phys.* **2005**, *122*, 224307.
(13) Aguado, A.; Barragán, P.; Prosmiti, R.; Delgado-Barrio, G.; Villarreal, P.; Roncero, O. *J. Chem. Phys.* **2010**, *133*, 024306.
(14) Gerlich, D.; Herbst, E.; Roueff, E. *Planet. Space Sci.* **2002**, *50*, 1275.
(15) Štich, I.; Marx, D.; Parrinello, M.; Terakura, K. *J. Chem. Phys.* **1997**, *107*, 9482.
(16) Ohta, Y.; Ohta, J.; Kinugawa, K. *J. Chem. Phys.* **2004**, *121*, 10991.
(17) Acioli, P. H.; Xie, Z.; Braams, B. J.; Bowman, J. M. *J. Chem. Phys.* **2008**, *128*, 104318.
(18) Car, R.; Parrinello, M. *Phys. Rev. Lett.* **1985**, *55*, 2471.
(19) Chermette, H.; Razafinjanahary, H.; Carrion, L. *J. Chem. Phys.* **1997**, *107*, 10643.
(20) *Gaussian 03*, revision C.02; Gaussian, Inc.: Wallingford, CT, 2004.
(21) Müller, H.; Kutzelnigg, W. *Phys. Chem. Chem. Phys.* **2000**, *2*, 2061.
(22) Barragán, P.; Prosmiti, R.; Roncero, O.; Aguado, A.; Villarreal, P.; Delgado-Barrio, G. *J. Chem. Phys.* **2010**, *133*, 054303.
(23) Barbatti, M.; Jalbert, G.; Nascimento, M. A. C. *J. Chem. Phys.* **2000**, *113*, 4230.
(24) Ignacio, E. W.; Yamabe, S. *Chem. Phys. Lett.* **1998**, *287*, 563.
(25) Prosmiti, R.; Villarreal, P.; Delgado-Barrio, G. *J. Phys. Chem. A* **2003**, *107*, 4768.
(26) Barragän, P.; Prosmiti, R.; Villarreal, P.; Delgado-Barrio, G. *Int. J. Quantum Chem.* **2011**, *111*, 368.
(27) Feyman, R. P.; Hibbs, A. R. *Quantum Mechanics and Path Integrals*; McGraw-Hill: New York, 1965.
(28) Ceperley, D. M. *Rev. Mod. Phys.* **1995**, *67*, 279.
(29) Glaesemann, K. R.; Fried, L. E. *J. Chem. Phys.* **2005**, *123*, 034103.
(30) Takahashi, M.; Imada, M. *J. Phys. Soc. Jpn.* **1984**, *53*, 3765.
(31) Brualla, L.; Sakkos, K.; Boronat, J.; Casulleras, J. *J. Chem. Phys.* **2004**, *121*, 636.
(32) Sakkos, K.; Casulleras, J.; Boronat, J. *J. Chem. Phys.* **2009**, *130*, 204109.
(33) Sprik, M.; Klein, M. L.; Chandler, D. *Phys. Rev. B* **1985**, *31*, 4234.
(34) Metropolis, N.; Rosenbluth, M. N.; Teller, A. H.; Teller, E. *J. Chem. Phys.* **1953**, *21*, 1087.
(35) Baker, J. A. *J. Chem. Phys.* **1979**, *70*, 2914.
(36) Herman, M. F.; Bruskin, E. J.; Berne, B. J. *J. Chem. Phys.* **1982**, *76*, 5150.
(37) Cao, J.; Berne, B. J. *J. Chem. Phys.* **1989**, *91*, 6359.
(38) Barragán, P.; Pérez de Tudela, R.; Prosmiti, R.; Villarreal, P.; Delgado-Barrio, G. *Phys. Scr.* **2011**, submitted.
(39) Barbatti, M.; Nascimento, M. A. C. *J. Chem. Phys.* **2003**, *119*, 5444.
(40) Gu, C.; Gao, G.-H. *Phys. Chem. Chem. Phys.* **2002**, *4*, 4700.